The jet-powered optical nebula of Cygnus X–1

D. M. Russell,[1]★ R. P. Fender,[1] E. Gallo[2]† and C. R. Kaiser[1]

[1]*School of Physics & Astronomy, University of Southampton, Highfield, Southampton SO17 1BJ*
[2]*Department of Physics, University of California, Santa Barbara, CA 93106, USA*

ABSTRACT

We present Hα and [O III] (5007 Å) images of the nebula powered by the jet of the black hole candidate and microquasar Cygnus X–1, observed with the 2.5-m Isaac Newton Telescope (INT). The ring-like structure is luminous in [O III] and there exists a thin outer shell with a high [O III]/Hα flux ratio. This outer shell probably originates in the collisionally excited atoms close to the front of the bow shock. Its presence indicates that the gas is shock excited as opposed to photoionized, supporting the jet-powered scenario. The shock velocity was previously constrained at $20 < v_s < 360$ km s^{-1}; here we show that $v_s \geqslant 100$ km s^{-1} (1σ confidence) based on a comparison of the observed [O III]/Hα ratio in the bow shock with a number of radiative shock models. From this we further constrain the time-averaged power of the jet: $P_{\rm Jet} = (4–14) \times 10^{36}$ erg s^{-1}. The Hα flux behind the shock front is typically 4×10^{-15} erg s^{-1} cm^{-2} arcsec^{-2}, and we estimate an upper limit of $\sim 8 \times 10^{-15}$ erg s^{-1} cm^{-2} arcsec^{-2} (3σ) to the optical (*R*-band) continuum flux of the nebula. The inferred age of the structure is similar to the time Cyg X–1 has been close to a bright H II region (due to the proper motion of the binary), indicating a dense local medium is required to form the shock wave. In addition, we search a >1 deg^2 field of view to the south of Cyg X–1 in Hα (provided by the INT Photometric Hα Survey of the Northern Galactic Plane; IPHAS) for evidence of the counter jet interacting with the surrounding medium. Two candidate regions are identified, whose possible association with the jet could be confirmed with follow-up observations in [S II] and deeper observations in [O III] and radio.

Key words: accretion, accretion discs – black hole physics – shock waves – stars: individual: Cygnus X-1 – ISM: jets and outflows – X-rays: binaries.

1 INTRODUCTION

Galactic black holes release an unknown fraction of their accreting matter and energy in the form of collimated outflows (or jets) that travel into the surrounding medium (for a review see Fender 2006). These accreting black hole candidate X-ray binaries (BHXBs) spend a large fraction of their lifetimes in a 'hard' X-ray state (Homan & Belloni 2005; McClintock & Remillard 2006) which is ubiquitously associated with the formation of partially self-absorbed synchrotron emitting radio jets (e.g. Fender, Belloni & Gallo 2004). While the presence of these jets is commonly inferred from a flat radio-through-infrared spectral component, radio observations of the nearby ($d = 2.1 \pm 0.1$ kpc; Massey, Johnson & Degioia-Eastwood 1995) high-mass BHXB Cygnus X–1 have directly resolved a collimated jet $\sim$30 au in length (Stirling et al. 2001), whilst in this X-ray state. A transient radio jet has also been observed of

length $\sim$140 au that was launched during a period of X-ray state transitions (Fender et al. 2006). Transient jets with high Lorentz factors are sometimes seen when a BHXB leaves the hard state (e.g. Fender et al. 2004).

The power carried by the self-absorbed, steady hard state jets when averaged over their lifetime stands as one of the key questions in our understanding of BHXB accretion, and possibly for black hole accretion on all mass scales. In recent years it has become apparent that a significant fraction of the liberated accretion power is ejected as outflows in hard state BHXBs (e.g. Gallo, Fender & Pooley 2003), and it now seems likely that in hard X-ray states the accretion flow is 'jet-dominated' (Fender, Gallo & Jonker 2003), with more power in the jets than in X-rays. Clearly, measuring as accurately as possible the jet power is key to understanding both the overall physics of the accretion process and the matter and energy input from BHXBs into the interstellar medium (ISM).

Attempts at estimating the jet power content from core radio luminosities are riddled with assumptions about its spectrum and radiative efficiency, the latter of which is poorly constrained (e.g. Ogley et al. 2000; Fender 2001; Homan et al. 2005; Heinz 2006). The jet

★E-mail: davidr@phys.soton.ac.uk
†*Chandra* Fellow.

power estimated in this way is highly sensitive to the location of the high-frequency break of the flat (spectral index $\alpha \approx 0$ where $F_\nu \propto \nu^\alpha$) optically thick part of the jet spectrum, as the radiative power is dominated by the higher energy photons (Blandford & Königl 1979). This break is likely to be at $\sim 2\,\mu$m, at least for BHXBs at high luminosities ($L_X \gtrsim 10^{36}$ erg s^{-1}) in the hard state (Corbel & Fender 2002; Nowak et al. 2005; Russell et al. 2006).

The jet power may alternatively be constrained by analysing its interaction with the surrounding medium, without requiring prior knowledge of the jet spectrum and radiative efficiency. Radio lobes associated with jets from active galactic nuclei (AGN) are commonly used as accurate calorimeters of the *power × lifetime* product of the jets (Burbidge 1959), a method only very recently applied to jets from stellar mass black holes. Radio lobes have been identified and associated with an increasing number of BHXBs (Mirabel et al. 1992; Rodríguez, Mirabel & Martí 1992; Corbel et al. 2002) and even a couple of neutron star X-ray binaries (Fomalont, Geldzahler & Bradshaw 2001; Tudose et al. 2006).

Recently, deep radio observations of the field of Cyg X–1 resulted in the discovery of a shell-like structure which is aligned with the aforementioned resolved radio jet (Gallo et al. 2005). This *jet-blown nebula* with a diameter of ~ 5 pc is interpreted as the result of a strong shock that develops at the location where the collimated jet impacts on the ambient ISM. The nebula was subsequently observed at optical wavelengths by the Isaac Newton Telescope (INT) Wide Field Camera (WFC) and is clearly visible in Hα (6568 Å) line emission, and coincident with the radio shell. The Hα flux density $F_\nu \geqslant 0.02$ mJy arcsec^{-2} is $\geqslant 20$ times the measured radio flux density, inconsistent with optically thin synchrotron emission between the two spectral regimes and instead favouring a thermal plasma (Gallo et al. 2005).

Models of X-ray binary jet–ISM interactions predict a shell of shocked compressed ISM emitting bremsstrahlung radiation containing a bubble of relativistic synchrotron-emitting plasma (Kaiser et al. 2004). As with any interstellar shock wave where the pre-shock gas is at least partially ionized by the approaching radiation field, line emission from recombination of the shocked gas is also expected (e.g. Cox 1972). The shell, which is essentially a radiative shock wave, consists of a bow shock front where the gas is in transition to a higher temperature due to collisions and plasma instabilities (e.g. McKee & Hollenbach 1980). The post-shocked gas then enters the optically thin 'cooling region', where the overall ionization level rises then falls as the gas radiatively cools to $\sim 10^4$ K (e.g. Cox & Raymond 1985). Shock waves are commonly observed in supernova remnants (SNRs), and shocks created from outflows exist in Herbig–Haro objects, where emission lines are produced in the shock wave created by bipolar flows from pre-main-sequence stars impacting the ISM (e.g. Schwartz 1983). Shock fronts associated with AGN jets interacting with the intracluster gas (which is much hotter than the ISM) are also seen at X-ray energies (Carilli, Perley & Harris 1994; Kraft et al. 2003; Forman et al. 2005; Nulsen et al. 2005; Croston, Kraft & Hardcastle 2006; Wilson, Smith & Young 2006). In addition, infrared sources found symmetric about the position of the X-ray binary GRS 1915+105 (Chaty et al. 2001) may be jet–ISM impact sites (Kaiser et al. 2004).

By modelling the shell emission of the Cyg X–1 nebula as originating from radiatively shocked gas (Castor, McCray & Weaver 1975; Kaiser & Alexander 1997; Heinz, Reynolds & Begelman 1998), the total power carried by the jet was estimated to be $\sim 9 \times 10^{35} \leqslant P_{\rm Jet} \leqslant 10^{37}$ erg s^{-1} which, when taking into account the power of the counter jet, is equal to ~ 0.06–1 times the bolometric X-ray luminosity of Cyg X–1 (Gallo et al. 2005). These calculations

have led to estimates of the matter content of the jet (Heinz 2006); a similar technique to those applied to the jets of AGN, where their matter content are inferred from a combination of information from the core and lobes (e.g. Celotti & Fabian 1993; Dunn, Fabian & Celotti 2006).

These jet power calculations are highly sensitive to the velocity of the gas in the shock front. From temperature constraints and from the non-detection of an X-ray counterpart, this was estimated to be $20 \leqslant v_{\rm s} \leqslant 360$ km s^{-1}. Emission line ratios of shock-heated gas can constrain its parameters, including the velocity of the shock (e.g. Osterbrock 1989).

Here, we performed wide field imaging observations of the region of Cyg X–1 in Hα and [O III] (5007 Å) filters in order to (i) constrain the velocity and temperature of the shocked gas and hence the time-averaged power of the X-ray binary jet of Cyg X–1, (ii) obtain for the first time flux-calibrated optical emission line measurements from a nebula powered by an X-ray binary jet and (iii) search for any jet–ISM interactions associated with the counter jet supposedly to the south of Cyg X–1.

2 OBSERVATIONS AND DATA REDUCTION

The field of Cyg X–1 and of two Landolt standard stars were observed using the WFC on the 2.5-m INT in narrowband and broadband filters. The images were taken on 2005 October 10 as part of a Galactic survey of emission line nebulae powered by X-ray binary jets (Russell et al., in preparation). The conditions were cloudless with a seeing of ~ 1–2 arcsec. The moon was set, making it possible to achieve a higher signal-to-noise ratio (S/N) than previous images presented in Gallo et al. (2005). Table 1 lists the observations used for this work. The WFC consists of four CCDs of 2048×4100 imaging pixels, each of scale 0.333 arcsec pixel^{-1}. The field of view is 34×34 arcmin^2.

Data reduction was performed using the pipeline package THELI (details in Erben et al. 2005). After manually separating the data into type (bias/flat/science) and filter, THELI debiased and flat-fielded the science frames. The package read the exposure time and right ascension (RA) and declination (Dec.) from the FITS file headers (it is currently configured for reducing data from ~ 30 instruments including the INT WFC) and matched several hundred stars in each exposure with those in the online MAST Guide Star Catalogue (release 2.2). THELI then aligned and stacked (for each position and filter) the images, and position-calibrated mosaics were created, with flux in counts s^{-1} pixel^{-1}. The resulting Hα and [O III] mosaics of the Cyg X–1 field are displayed in Fig. 1.

3 FLUX CALIBRATION

The Landolt standard stars 94–171 ($V = 12.659$; $R = 12.179$) and 94–702 ($V = 11.594$; $R = 10.838$) were observed at low airmass (see Table 1). We performed aperture photometry of the standards in the V- and R-band reduced images with PHOTOM and accounted for airmass-dependent atmospheric extinction according to King (1985). The resulting conversion between intrinsic flux density (at airmass = 0) and counts s^{-1} differed between the two standards by a factor of 0.5 and 6.5 per cent for V and R, respectively. The Hα filter is located within the passband of the Harris R filter, and [O III] is located within the Harris V filter. For a flat spectrum source, the WFC R-band filter collects 15.742 times more flux than the Hα filter, and likewise V collects 11.127 times more flux than [O III]. By multiplying by these factors we obtain 7.140×10^{-3} mJy

Table 1. List of observations with the INT WFC.

Run no.	MJD	Target	RA and Dec. (centre of CCD 4; J2000)	Airmass	Filter	Exposure time (s)
473434	53653.922	Cyg X–1 north	19 59 38.49 +35 18 20.0	1.171	[O III] 5007 Å	1200
473435	53653.937	Cyg X–1 north	19 59 39.31 +35 18 29.6	1.231	[O III] 5007 Å	1200
473436	53653.956	Cyg X–1 north	19 59 38.50 +35 18 20.0	1.310	Harris V	600
473437	53653.963	Cyg X–1 north	19 59 38.49 +35 18 20.0	1.380	Hα 6568 Å	1200
473438	53653.978	Cyg X–1 north	19 59 39.31 +35 18 30.0	1.494	Hα 6568 Å	1200
473439	53653.996	Cyg X–1 north	19 59 37.68 +35 18 10.0	1.620	Harris R	600
473441	53654.013	Cyg X–1 south	19 59 07.99 +34 56 59.9	1.860	[O III] 5007 Å	900
473442	53654.025	Cyg X–1 south	19 59 08.80 +34 57 09.8	2.064	[O III] 5007 Å	900
473452	53654.106	Landolt 94–171	02 53 38.80 +00 17 17.9	1.139	Harris R	10
473454	53654.109	Landolt 94–171	02 53 38.79 +00 17 18.0	1.138	Harris V	10
473457	53654.113	Landolt 94–702	02 58 13.39 +01 10 54.0	1.128	Harris V	10
473458	53654.113	Landolt 94–702	02 58 13.39 +01 10 53.9	1.128	Harris R	10

The positions refer to the centre of CCD 4, which is the middle of the three eastern CCDs (Fig. 1). 10 bias frames and $5 \times$ Hα, $7 \times$ [O III] 5007 Å, $6 \times$ Harris R-band and $5 \times$ Harris V-band sky flats were taken in the same observing night.

(intrinsic) per counts s^{-1} for Hα and 5.637×10^{-3} mJy (intrinsic) per counts s^{-1} for [O III].

As a check of our calibration, we measured the fluxes of 10 stars in our reduced Cyg X–1 Hα image, that are listed in the INT Photometric Hα Survey of the Northern Galactic Plane (IPHAS; Drew et al. 2005) catalogue (which uses the same telescope, instrument and filter). The ratio of the Hα flux of each star measured here to that listed in the catalogue is 1.06 ± 0.39 (1σ). We can therefore assume our flux calibration is accurate, and we adopt a 1σ error for each flux measurement F (Hα and [O III]), of 0.14 dex (i.e. log $F \pm$ 0.14).

We created flux-calibrated continuum-subtracted Hα and [O III] images of the region of Cyg X–1 (Figs 2a and b) using IMUTIL and IMMATCH in IRAF. The resulting images are corrected for interstellar extinction towards Cyg X–1 adopting $A_V = 2.95 \pm 0.21$ (Wu et al. 1982). The extinction towards Cyg X–1 and its nebula may vary over the field of view. The total neutral hydrogen column density N_H through the Galaxy at various positions in a ~ 4 deg^2 area around Cyg X–1 (Hartmann & Burton 1997) is indicated in Fig. 3. N_H appears to vary smoothly over the field, and the four closest points to Cyg X–1 yield $N_H = (6.55 \pm 0.94) \times 10^{21}$ cm^{-2} in the region containing Cyg X–1, or $A_V = 3.66 \pm 0.53$ adopting $N_H = 1.79 \times 10^{21}$ cm^{-2} A_V (Predehl & Schmitt 1995). If the extinction A_V towards Cyg X–1 (i.e. not through the whole Galaxy in this direction) also varies by ± 0.53 over the much smaller field of view of the nebula (a conservative case), an error is introduced of 0.18 and 0.25 dex to the Hα and [O III] flux measurements, respectively (no distance estimate is required). The measurements of [O III]/Hα however only suffer a 0.06 dex uncertainty due to the different extinctions suffered at the two wavelengths ([O III] at 5007 Å and Hα at 6568Å; this concerns only the contribution to the error budget of the extinction).

Propagating the above two sources of error, we arrive at

$$\Delta(\log_{10} F_{Hα}) = 0.23 \log_{10} F_{Hα}, \tag{1}$$

$$\Delta(\log_{10} F_{[O III]}) = 0.29 \log_{10} F_{[O III]}, \tag{2}$$

$$\Delta(\log_{10}(F_{[O III]}/F_{Hα})) = 0.15 \log_{10}(F_{[O III]}/F_{Hα}). \tag{3}$$

[O III]/Hα and R-band–Hα images were also created (Figs 2c and d). The [O III]/Hα image represents the ratio of the [O III] and Hα fluxes (in dereddened erg s^{-1} cm^{-2} arcsec^{-2}) and the Hα contribu-

tion is subtracted from the continuum in the R-band–Hα image. The 1.4-GHz radio image of Gallo et al. (2005) in shown in Fig. 2(e) for comparison.

4 RESULTS

The Hα and [O III] fluxes measured in a number of positions in the shell of the nebula are plotted in Fig. 4. It seems that the [O III]/Hα ratio increases with position going clockwise around the shell, from values of $F_{[O III]}/F_{Hα} \sim 0.2$ on the eastern side to ~ 1.2 on the western side of the nebula. The fluxes of both emission lines are also higher on the western side. The line ratio is approximately constant in the filaments inside the nebula, with values of $F_{[O III]}/F_{Hα} \sim 0.7$. The H II region Sh2–101 and the 'stream' of diffuse emission joining the region to the Cyg X–1 nebula, possess ratios of order $F_{[O III]}/F_{Hα} \sim$ 0–0.2, with one area (RA 19 59 45, Dec. +35 18 48) having a higher value, $F_{[O III]}/F_{Hα} \sim 0.6$. This area resembles a shell-like feature close to a bright star HD 227018 at the centre of the H II region, and could be a bow shock associated with the motion of this star (which is 12 mas yr^{-1} in the direction of the observed shell in the H II region; Perryman et al. 1997). We measure the flux in the H II region to be $F_{Hα} \sim 5$–15×10^{-14} erg s^{-1} cm^{-2} arcsec^{-2} ; $F_{[O III]} \sim 0.5$–5×10^{-14} erg s^{-1} cm^{-2} arcsec^{-2}.

The large quantity of stars in the line of sight of the shell prevent us from accurately calculating the total Hα and [O III] luminosity of the structure. However, we can conservatively estimate the area of the emitting gas to be between 3 arcmin^2 (approximating the nebula to a 15×700-arcsec^2 area) and 46 arcmin^2 (the area of a circle with radius 4 arcmin) and take the mean flux of the nebula (Fig. 4) to constrain its luminosity. At a distance of 2.1 kpc, the Hα and [O III] luminosities of the nebula are $1.8 \times 10^{34} \leqslant L_{Hα} \leqslant 2.8 \times 10^{35}$ erg s^{-1} and $1.3 \times 10^{34} \leqslant L_{[O III]} \leqslant 2.1 \times 10^{35}$ erg s^{-1}, respectively.

In 10 regions (of ~ 5 arcsec^2 areas) inside and outside the Hα-emitting nebula, the R-band dereddened Hα-subtracted flux is consistent with zero, and the mean of the s.d. values in each region is 2.57×10^{-15} erg s^{-1} cm^{-2} arcsec^{-2}. We therefore have a 3σ upper limit to the R-band flux of 7.7×10^{-15} erg s^{-1} cm^{-2} arcsec^{-2}, or a flux density of 0.0068 mJy arcsec^{-2}. Similarly, we obtain a 3σ upper limit to the V-band flux (from $10 \sim 5$ arcsec^2 regions) of 2.0×10^{-14} erg s^{-1} cm^{-2} arcsec^{-2} or 0.0196 mJy arcsec^{-2}. From the R-band upper limit, we conclude that the optical continuum flux
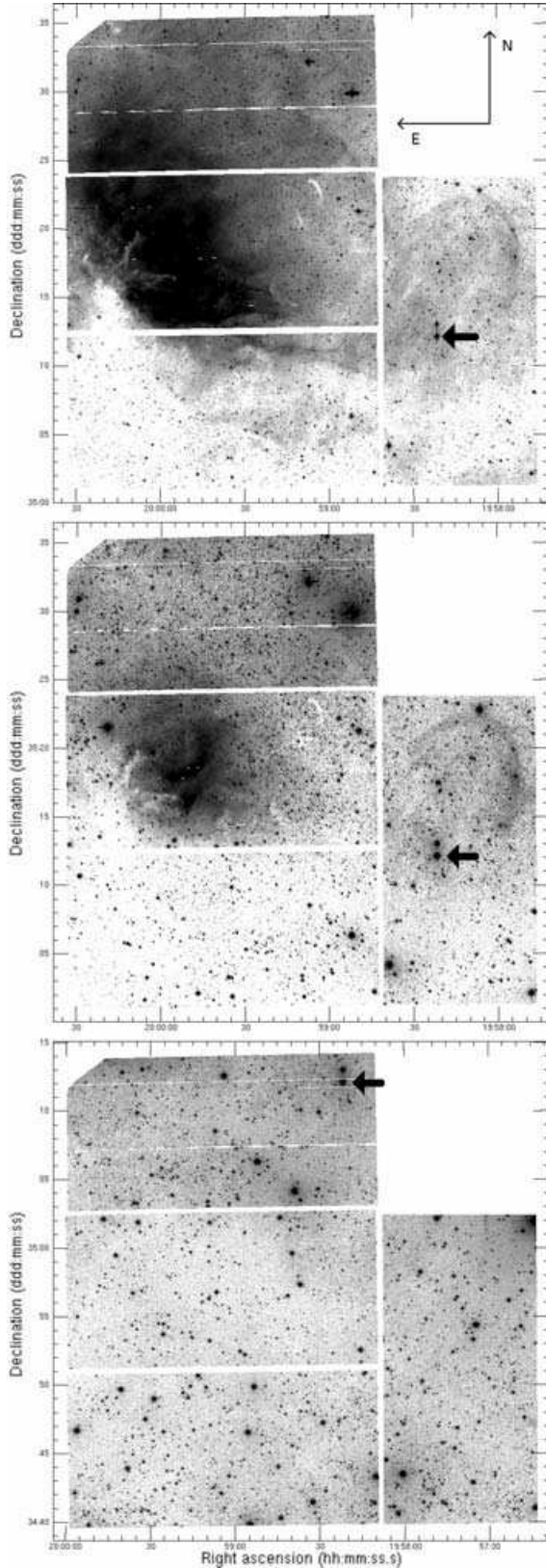
Figure 1. Stacked WFC images of the field of Cyg X–1. Top: 2400 s in Hα (6568 Å); centre: 2400 s in [O III] (5007 Å); lower: 1800 s [O III] (5007 Å) of the field south of Cyg X–1. Cyg X–1 is indicated by an arrow in each panel. In the top and middle panels, the H II region Sh2–101 is prominent on the eastern CCD chips and the Cyg X–1 shell nebula is visible to the north-west of the system.

density is $\leqslant 7$ times the radio flux density (Gallo et al. 2005), yielding a radio–optical spectral index $\alpha \leqslant 0.15$.

The broadband spectrum is consistent with bremsstrahlung emission with a flat radio–optical continuum and optical emission lines which are at least one order of magnitude more luminous than the continuum. We cannot however definitely state that the radio emission is thermal in origin, as mixed thermal/non-thermal plasma is seen in some environments (e.g. the arcsec-scale jets of SS 433; Migliari et al. 2002). A future measurement of the radio spectral index, which is difficult to achieve, is required to test whether the radio through optical spectrum is consistent with a thermal plasma or requires two (or more) components. Currently the morphology of the radio emission, being spatially coincident with the rather thin optical shell, does seem to favour the single thermal plasma model.

4.1 Morphology and nature of the nebula

The higher S/N in the Hα image compared to that in Gallo et al. (2005) is striking from the observed structure within the nebula (Fig. 2a). One would expect the most luminous areas of the nebula to occur in regions of the shock front where the line of sight is tangential to its surface and therefore should exist only at the apparent edge of the nebula if the structure is spherical. Filaments of gas are seen within the nebula and are unlikely to originate in unassociated line-of-sight photoionized gas because of their filamental morphology; the nebulosity is less diffuse than the gas in the photoionized H II region. The [O III]/Hα ratios of ∼0.7 in the filaments and morphology suggest either multiple shock fronts or an uneven non-spherical nebula. The latter is expected for a varying pre-shock gas density, which is clearly the case on inspection of the variation in Hα nebulosity close to the nebula.

The [O III]/Hα image reveals two striking features: first, the Hα nebulosity (which extends from the H II region Sh2–101 to the east of the nebula) possesses a low [O III]/Hα flux ratio compared to the Cyg X–1 nebula, and secondly there exists a thin outer shell to the Cyg X–1 nebula with a higher [O III]/Hα ratio. H II regions and photoionized gas in general can possess a wide range of [O III]/Hα ratios (e.g. Johnson 1953; Blair, Kirshner & Chevalier 1982) but this morphology of an outer [O III]-emitting shell is only expected from shock-excited gas. These two observations confirm that the gas in the Cyg X–1 nebula must be ionized by a different source to the surrounding nebulosity.

In Fig. 5 we show a blow-up of the north-west area of the nebula in [O III]/Hα; clearly showing this thin shell of enhanced [O III]/Hα ratio on the outer side of the ring. We have taken a 3.3 arcsec-wide slice through the image (indicated in Fig. 5) and plot the emission line flux and $F_{[O III]}/F_{Hα}$ flux ratio along this slice in Fig. 6. The upper panel of Fig. 6 shows that there is a sharp outer edge to the ring, and this edge is further out in [O III] than in Hα. This results in the thin outer shell of enhanced [O III]/Hα ratio that is visible in the lower panel of Fig. 6. This outer shell is ∼6 arcsec thick and the rest of the ring is ∼40 arcsec thick, at least in the region of the slice. We note that the thin shell of enhanced [O III]/Hα ratio is not due to inaccurate alignment of the [O III] and Hα images as the stars are aligned and the thin shell exists on both sides of the nebula.

4.2 Constraining the shock velocity and jet power

We measured the $F_{[O III]}/F_{Hα}$ flux ratio in seven 'slices' (typical thickness 12 pixels = 4 arcsec) of the [O III]-emitting shock front, and in four larger regions behind it. In the thin outer shell we obtain $F_{[O III]}/F_{Hα} = 1.36 \pm 0.28$ and behind the shell, $F_{[O III]}/F_{Hα} =$
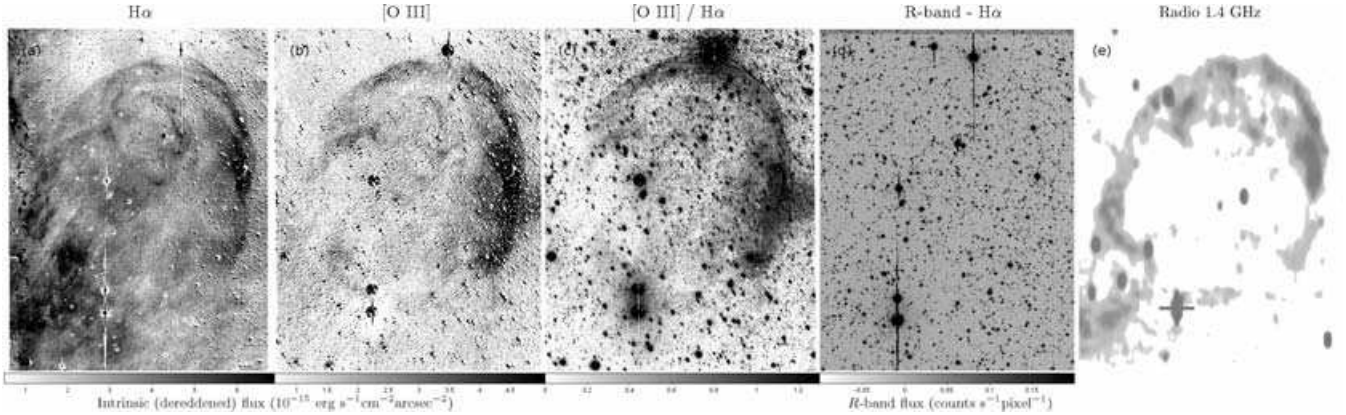
Figure 2. Images of the Cyg X–1 ring nebula in (a) Hα; (b) [O III]; (c) [O III]/Hα; (d) R-band–Hα and (e) radio 1.4 GHz (Gallo et al. 2005). The Hα and [O III] images are dereddened using $A_V = 2.95$ measured for Cyg X–1 (Wu et al. 1982), flux calibrated and continuum-subtracted (i.e. Hα − R and [O III] − V). The [O III]/Hα flux ratio image is created from the non-continuum-subtracted [O III] and Hα frames. The Hα contribution has been subtracted from the R-band image on the extreme right-hand panel, in which the nebula is not visible. Cyg X–1 is the lower of the two bright stars near the bottom of each image and is marked by a cross in the radio image.
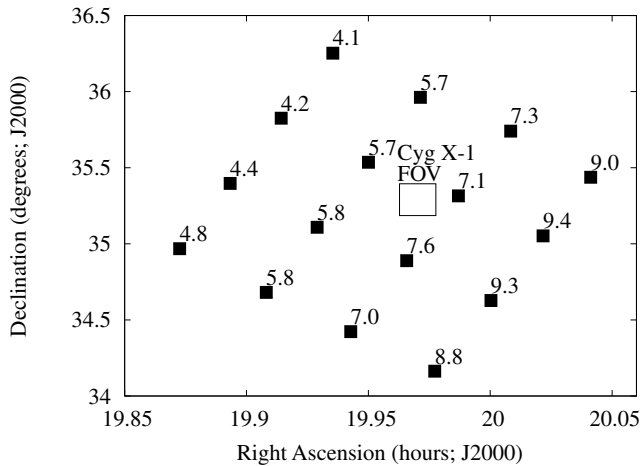
Figure 3. Total Galactic neutral hydrogen column density N_H in units of 10^{21} cm^{-2} at positions close to Cyg X–1 (Hartmann & Burton 1997). The box indicates the field of view (FOV) containing Cyg X–1 and its nebula.

0.89 ± 0.46. Taking into account the error from equation 3, $F_{[O III]}/H_\alpha = 1.36^{+0.65}_{-0.46}$ in the shock front and $F_{[O III]}/H_\alpha = 0.89^{+0.64}_{-0.49}$ in the nebula behind the shock front.

Both radiative and non-radiative shock waves are expected to produce a mix of line (radiative recombination) and continuum (due to bremsstrahlung emission) output (e.g. Krolik 1999). Non-radiative shock waves (defined as when the cooling time of the shocked gas exceeds the age of the shock) produce Balmer optical emission lines only, because the heavier atoms are not excited (e.g. McKee & Hollenbach 1980), so the existence of the strong [O III] line confirms the radiative nature of the Cyg X–1 nebula shock. In a radiative bow shock, the ambient ISM gas is first perturbed by the approaching radiation field. The ionization of pre-shock hydrogen becomes progressively more significant in the velocity range $90 \leqslant v_s \leqslant 120$ km s^{-1}; below 90 km s^{-1} the pre-shock gas is essentially neutral and above 120 km s^{-1} it is entirely ionized (e.g. Shull & McKee 1979). In addition, at velocities ~100 km s^{-1} the ionizing He II (304Å) photons from the cooling region can doubly ionize the oxygen increasing the intensity of the [O III] lines (McKee &

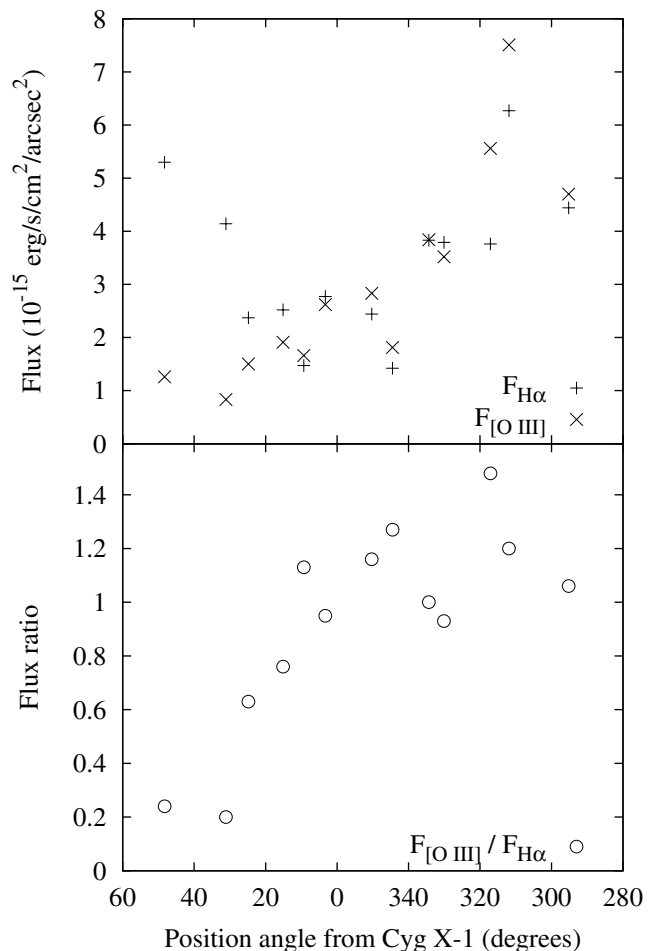**Figure 4.** Intrinsic dereddened continuum-subtracted Hα and [O III] fluxes at various positions around the shell, versus the position angle from Cyg X–1. See equations (1)–(3) for the errors associated with each flux measurement. At each position, the mean flux in a 164-arcsec^2 circular aperture containing no visible stars is plotted. The data on the left-hand side are from the eastern side of the nebula and the data on the right-hand side are from the western side.
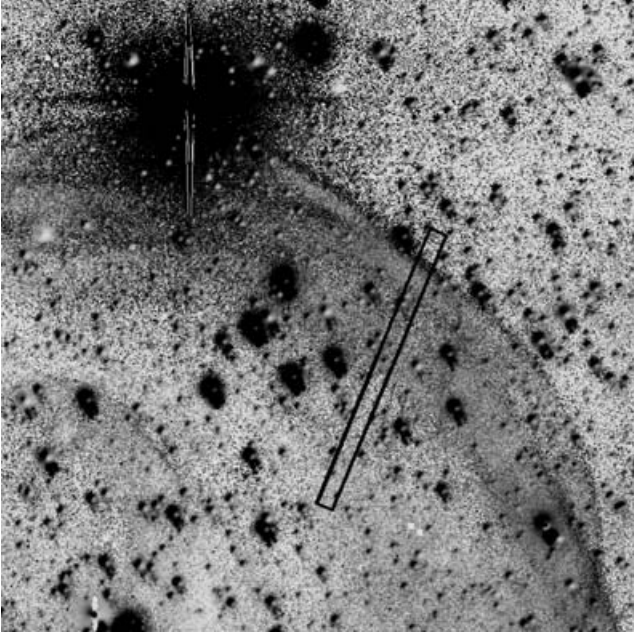
Figure 5. A blow-up of part of Fig. 2(c): [O III]/Hα image of the Cyg X–1 ring nebula. We interpret the thin outer shell with a high [O III]/Hα flux ratio as possibly originating in the ionized atoms close to the front of the bow shock. North is up, east is to the left-hand side. The emission line fluxes and [O III]/Hα ratio along the slice indicated in the image are shown in Fig. 6.

Figure 6. The emission line flux (upper panel) and the [O III]/Hα ratio (lower panel) along a slice through the nebula indicated in Fig. 5. The [O III] flux has been offset by -5×10^{-15} erg s^{-1} cm^{-2} arcsec^{-2} for clarity. In the lower panel, region a = inside the nebula; b = the ring nebula; c = the thin outer shell luminous in [O III]/Hα and d = outside the nebula. The mean error associated with each data set (equations 1–3) is indicated on the left-hand side in the panels. The spikes in the upper panel are due to stars in the slice.

Hollenbach 1980). This leads to the high excitation line [O III] becoming negligible at low velocities in all shock-wave models (Raymond 1979; Shull & McKee 1979; Dopita et al. 1984; Binette, Dopita & Tuohy 1985; Cox & Raymond 1985; Hartigan, Raymond & Hartmann 1987; Dopita & Sutherland 1995, 1996). The outer shell of the Cyg X–1 nebula, bright in [O III]/Hα, may originate in the ionized atoms close to the front of the bow shock, and its presence confirms its association with the jet of Cyg X–1.

Radiative shock models predict that relative optical line strengths of the shocked gas are highly sensitive to the temperature and velocity of the shock wave, and vary only weakly with the conditions in the pre-shock gas such as the elemental abundances (e.g. Cox & Raymond 1985). Temperatures and velocities of shocked matter, mainly in SNRs, are commonly inferred by comparing their observed optical or ultraviolet (UV) line ratios to these models (e.g. Blair et al. 1991; Vancura et al. 1992; Levenson et al. 1995; Bocchino et al. 2000; Mavromatakis et al. 2001). The bright [O III]/Hα shock front of the Cyg X–1 nebula appears to be thicker on the western side of the nebula, and the Hα and [O III] surface brightness is also higher in this region (Fig. 4). This implies the shock may be faster here, possibly due to a lower pre-shock density; it is the furthest area of the nebula from the H II region (or due to the proper motion of Cyg X–1; see below).

The relation between the shock velocity and [O III]/Hα ratio in the shell is described for most of the published models of steady-flow radiative shocks with self-consistent pre-ionization (Binette et al. 1985; Cox & Raymond 1985; Hartigan et al. 1987; Dopita & Sutherland 1995). The reliability of these models can be assessed from their level of agreement, unless there are systematic uncertainties common to all models (which seems not to be the case as the velocities predicted by the models are consistent with velocities observed using other methods; e.g. Michael et al. 2000; Pun et al. 2002). In Fig. 7 we plot the aforementioned relation predicted
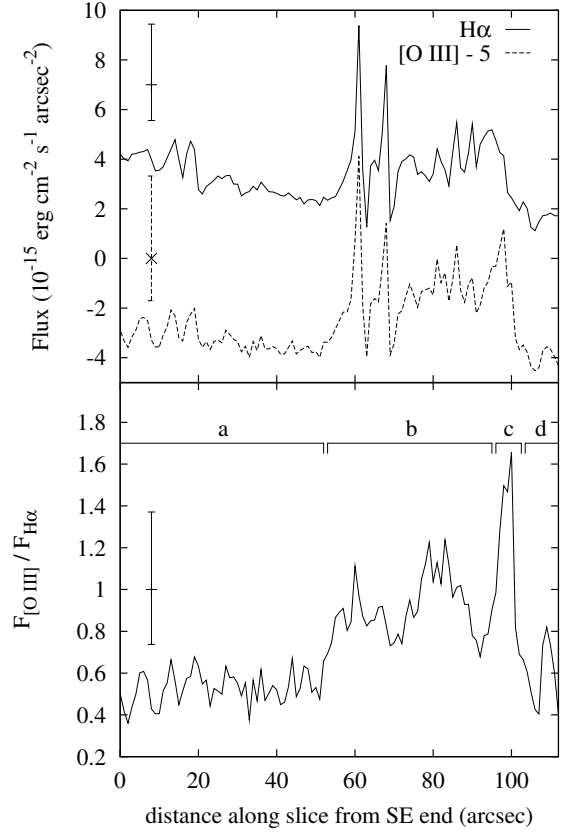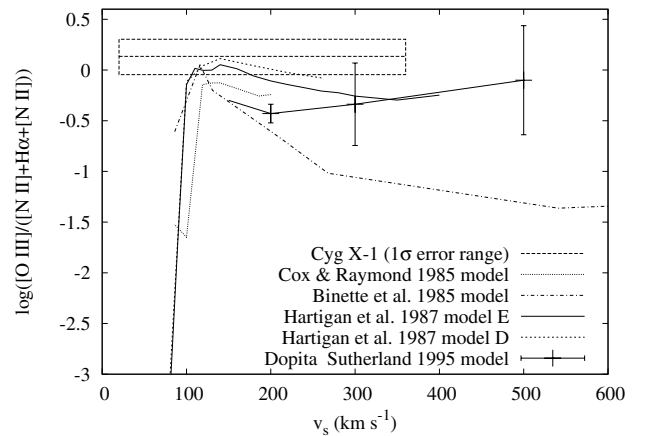

Figure 7. The [O III]/Hα ratio as a function of shock velocity predicted from five radiative shock models. The dashed rectangle represents the constrained range of values measured for the Cyg X–1 shock front (velocity range from Gallo et al. 2005). The INT [O III] filter includes both lines of the doublet; 4958.9 and 5006.9 Å, and the Hα filter includes the two [N II] lines at 6548.1 and 6583.4 Å in addition to 6562.8 Å Hα, within its bandpass. We therefore plot $\log(F_{[O III]+[O III]}/F_{[N II]+Hα+[N II]})$ versus velocity.

from five of the most advanced radiative shock models. We overplot the empirical [O III]/Hα ratio found for the Cyg X–1 shock front. Bearing in mind the previously estimated range of shock velocities, $20 < v_s < 360$ km s^{-1}, we find that outside the range $100 \leqslant v_s \leqslant 360$ km s^{-1}, no models successfully predict the observed [O III]/Hα measurement to within 1σ. Subsequently, we infer a temperature of the gas in the shocked shell (Gallo et al. 2005) of $2.4 \times 10^5 \leqslant T_s \leqslant 3.1 \times 10^6$ K. The models in Fig. 7 assume typical Galactic abundances and pre-shock particle densities within the range inferred for the Cyg X–1 nebula; $1 \leqslant n_0 \leqslant 300$ cm^{-3} (Gallo et al. 2005).

By constraining the velocity and temperature of the gas in the shock front, we are able to refine a number of parameters such as the particle density in the shell and power in the jet (Gallo et al. 2005). Table 2 lists the parameters inferred for the nebula and jet. We adopt the same methodology to calculate the parameters as used in Gallo et al. (2005). The temperature-dependent ionization fraction of the

Table 2. Revised nebula and jet parameters (1σ confidence limits where quoted).

Parameter	Value
Unchanged parameters (Gallo et al. 2005)	
Monochromatic radio luminosity	$L_{\nu,1.4\mathrm{GHz}} \approx 10^{18}$ erg s^{-1}Hz^{-1}
Cyg X–1 – shell separation	$L \approx 3.3 \times 10^{19}$ cm
Jet inclination angle to line of sight	$\theta \approx 35°$
Thickness of shell	$\Delta R \approx 1.6 \times 10^{18}$ cm
Source unit volume	$V(L, \Delta R) \approx 4 \times 10^{53}$ cm^3
Bremsstrahlung emissivity for hydrogen gas	$\epsilon_\nu(V, L_{\nu,1.4\mathrm{GHz}}) \approx 2.5 \times 10^{-36}$ erg s^{-1}Hz^{-1} cm^{-3}
Gaunt factor	$g \approx 6$
Number density of pre-shock gas	$1 \leqslant n_0 \leqslant 300$ cm^{-3}
Refined parameters	
Hα flux of shell	$F_{\mathrm{H}\alpha} \approx 3.6 \times 10^{-15}$ erg s^{-1}cm^{-2}arcsec^{-2}
Hα luminosity of nebula	$1.8 \times 10^{34} \leqslant L_{\mathrm{H}\alpha} \leqslant 2.8 \times 10^{35}$ erg s^{-1}
[O III] flux of shell	$F_{[\mathrm{O\,III}]} \approx 2.8 \times 10^{-15}$ erg s^{-1}cm^{-2}arcsec^{-2}
[O III] luminosity of nebula	$1.3 \times 10^{34} \leqslant L_{[\mathrm{O\,III}]} \leqslant 2.1 \times 10^{35}$ erg s^{-1}
[O III]/Hα ratio in shock front	$F_{[\mathrm{O\,III}]}/F_{\mathrm{H}\alpha} = 1.36^{+0.65}_{-0.46}$
[O III]/Hα ratio behind shock front	$F_{[\mathrm{O\,III}]}/F_{\mathrm{H}\alpha} = 0.89^{+0.64}_{-0.49}$
Optical continuum flux density of shell	$F_{\nu,\mathrm{OPT}} \leqslant 6.8$ μJy arcsec^{-2} (3σ)
Shock velocity	$100 \leqslant v_s \leqslant 360$ km s^{-1}
Shocked gas temperature	$2.4 \times 10^5 \leqslant T_s \leqslant 3.1 \times 10^6$ K
Number density of ionized particles in shell	$56 \leqslant n_e \leqslant 103$ cm^{-3}
Ionization fraction	$x \approx 1$
Number density of total particles in the shell	$56 \leqslant n_p \leqslant 103$ cm^{-3}
Jet lifetime	$0.017 \leqslant t \leqslant 0.063$ Myr
Time-averaged jet power	$P_{\mathrm{Jet}} = (4-14) \times 10^{36}$ erg s^{-1}
Hard state jet power including both jets	$P_{\mathrm{Jets}} = (9-30) \times 10^{36}$ erg s^{-1}
Outflow power/X-ray luminosity	$0.3 \leqslant f_{\mathrm{Jet/X}} \leqslant 1.0$

gas x is taken from Spitzer (1978). At the temperatures inferred, the hydrogen in the shocked shell is fully ionized. We have improved the accuracy of the shock velocity, the time-averaged jet power and the jet lifetime from > 1 to ~0.5 dex. Assuming the power originates in the hard state jet which is switched on for ~90 per cent of the lifetime of Cyg X–1 (e.g. Gallo et al. 2005), the total power of both these jets is between 30 and 100 per cent of the bolometric 0.1–200 keV X-ray luminosity ($L_X \approx 3 \times 10^{37}$ erg s^{-1}; Di Salvo et al. 2001).

Assuming the shock velocity has been approximately constant over the lifetime of the jet, the jet lifetime $t \sim 0.02$–0.06 Myr is much shorter than the estimated age of the progenitor of the black hole, ~5–7 Myr (Mirabel & Rodrigues 2003). However, given that the proper motion of Cyg X–1 is ~8.7 mas yr^{-1} in a direction ~130 degrees from the jet direction (Lestrade et al. 1999; Stirling et al. 2001; Mirabel & Rodrigues 2003), the system must have travelled between 2.5 and 9.1 arcmin during the lifetime of the jet. We speculate that the jet may have been present for the lifetime of Cyg X–1, but only when the system moved into the ISM close to the H II region did the local density become large enough for a bow shock to form. In fact, the age of the nebula (if it is powered by the jet) cannot exceed ~0.04 Myr because the position of Cyg X–1 at the birth of the jet would be *in front of* the bow shock. This scenario may also explain the apparent higher [O III]/Hα ratio and velocity of the gas on the western side of the nebula compared with the eastern side: the western side is further from the jet origin as the Cyg X–1 system moves.

4.3 Ruling out alternative origins of the shell

We have shown (Section 4.1) that the morphology of the Cyg X–1 nebula indicates the gas is shock-excited and not photoionized; the structure is therefore not a planetary nebula or an H II region. The nebula also cannot be a SNR associated with Cyg X–1 itself (Gallo et al. 2005). The proximity of the nebula to Cyg X–1, its alignment with the Cyg X–1 jet and the agreement of its age inferred from its velocity and from the proper motion of Cyg X–1 (Section 4.2) all point towards the jet-powered scenario. The one remaining alternative is a field SNR not associated with Cyg X–1; we here explore this possibility.

Xu, Zhang & Han (2005a) plot the diameter of 185 Galactic SNRs against their 1-GHz surface brightness (fig. 3 of that paper). The radio surface brightness of the Cyg X–1 nebula is $\Sigma_{1\,\mathrm{GHz}} \approx 3 \times 10^{-23}$ W m^{-2} Hz^{-1} sr^{-1} (lower than any SNR in the sample of Xu et al. 2005a), and would have a diameter of $\gtrsim 100$ pc if it were to lie close to the diameter–surface brightness relation for SNRs. The nebula has an angular diameter of ~7 arcmin, suggesting a distance to the source of $d \gtrsim 50$ kpc if it is a SNR. However, the authors note that this surface brightness–diameter relation could be severely biased by selection effects (Xu, Zhang & Han 2005b). Large, low surface-brightness SNRs may not have been detected in surveys due to confusion with strong foreground and background sources (e.g. Green 2004). We therefore cannot completely rule out a SNR origin to the nebula, but its alignment with the relativistic jet of Cyg X–1 (for example) strongly suggests it is related to the system.

4.4 The search for ISM interactions with the southern jet

We searched a ~0.25 deg^2 field in [O III] south of Cyg X–1 for a shell powered by the southern jet (lower panel of Fig. 1). No shell was observed in the 1800 s image, nor any visual nebulosity detected
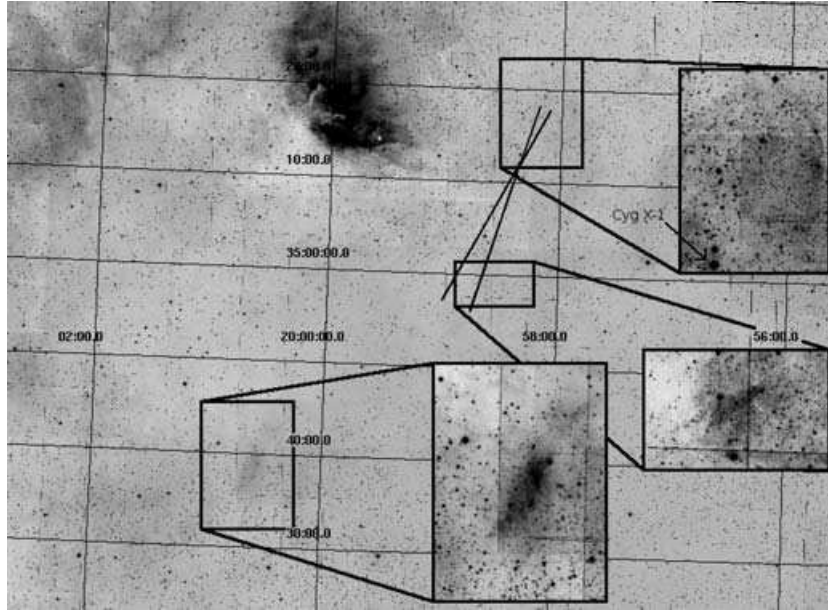
Figure 8. A ∼1.5-deg² mosaic from the IPHAS survey. Each CCD frame is a 120-s Hα exposure. North is to the top, east to the left-hand side. RA and Dec. are epoch J2000. The most extreme opening position angles of the resolved radio jet (both the steady low/hard state and transient jets) north of Cyg X–1; $17° \leqslant \theta \leqslant 28°$ (Stirling et al. 2001; Fender et al. 2006, also projected to the south assuming the jets are antiparallel) are shown. The north nebula and two areas of candidate ISM interactions with the southern jet of Cyg X–1 are expanded.

in the [O III] images that is consistent with the southern jet of Cyg X–1 interacting with the ISM. The mass density of ISM may be much less to the south; the jet should travel essentially ballistically and undetected until being decelerated by a denser region. Heinz (2002) found that the rarity of jet-powered lobes in microquasars compared to AGN is likely due to the lower density environment. In addition, it is interesting to note that the X-ray-bright shocked edges surrounding AGN radio lobes are sometimes one-sided (Kraft et al. 2003). We searched a ∼1-deg² Hα mosaic from the IPHAS survey (Drew et al. 2005, see Fig. 8). Two-candidate 'hot spots' analogous to those associated with AGN jets were identified, and are expanded in the figure.

Radio emission exists in the region close to the northern hot spot according to Martí et al. (1996), but it is uncertain whether it originates in point sources or extended emission. We inspected the southern region of the 1.4 GHz radio image obtained by Gallo et al. (2005) to search for diffuse emission. In a 1600×1600-arcsec² region close to the more northern Hα hot spot (the southern hot spot is not within the radio field of view), the mean rms flux density is 4×10^{-4} Jy beam⁻¹, yielding a 3σ upper limit to the (putative) radio hot spot in that region of 1.2 mJy beam⁻¹. Deeper radio observations are needed to test whether the candidate Hα hot spots have radio counterparts, as would be expected if they are jet–ISM interaction sites. In addition, observations in [S II] would test whether the emitting gas is shock-excited or photoionized, and deeper [O III] observations may constrain the velocity of any shocked gas.

5 CONCLUSIONS

We have imaged the shell-like nebula supposedly powered by the jet of Cyg X–1 in narrowband optical emission line filters. The nebula is bright in Hα and [O III] and the morphology and line ratios indicate that it is a radiative shock wave with a velocity $v_s \geqslant 100$ km s⁻¹. We rule out alternative interpretations of the structure such as photoionized gas, but cannot completely rule out an unre-

lated SNR origin. However, the morphology of the nebula and its alignment with the jet of Cyg X–1 strongly suggest that it is indeed powered by this jet. We have probably isolated for the first time the thin, hot, compressed gas close to the bow shock front of a nebula powered by an X-ray binary jet. The time-averaged power of the jet must be $P_{Jet} = (4–14) \times 10^{36}$ erg s⁻¹ to power a shock wave of the inferred size, luminosity, velocity and temperature. If the steady hard state jet of Cyg X–1 (i.e. active for ∼90 per cent of the time) is providing this power (rather than the transient jet; Fender et al. 2006), the total energy of both jets in the hard state is 0.3–1.0 times the bolometric X-ray luminosity. This provides the strongest evidence so far that at an accretion rate of ∼2 per cent Eddington, Cyg X–1 is in a state of approximate equipartition between radiative and kinetic output. Lower accretion rates should therefore be jet-dominated (Fender et al. 2003; Körding, Fender & Migliari 2006). The inferred age of the nebula is consistent with the time Cyg X–1 has been close to the currently nearby H II region.

No nebula associated with the southern jet of Cyg X–1 is observed, although we detect two putative Hα 'hot spots' that require optical emission line and radio follow-up to confirm their nature. Optical and UV (e.g. Blair et al. 1991) spectra of the northern shell will provide invaluable insights into the properties of the shocked gas, and hence the jet.

REFERENCES

Binette L., Dopita M. A., Tuohy I. R., 1985, ApJ, 297, 476
Blair W. P., Kirshner R. P., Chevalier R. A., 1982, ApJ, 254, 50
Blair W. P. et al., 1991, ApJ, 379, L33
Blandford R. D., Königl A., 1979, ApJ, 232, 34
Bocchino F., Maggio A., Sciortino S., Raymond J., 2000, A&A, 359, 316
Burbidge G. R., 1959, ApJ, 129, 849
Carilli C. L., Perley R. A., Harris D. E., 1994, MNRAS, 270, 173
Castor J., McCray R., Weaver R., 1975, ApJ, 200, L107
Celotti A., Fabian A. C., 1993, MNRAS, 264, 228
Chaty S., Rodríguez L. F., Mirabel I. F., Geballe T. R., Fuchs Y., Claret A., Cesarsky C. J., Cesarsky D., 2001, A&A, 366, 1035
Corbel S., Fender R. P., 2002, ApJ, 573, L35
Corbel S., Fender R. P., Tzioumis A. K., Tomsick J. A., Orosz J. A., Miller J. M., Wijnands R., Kaaret P., 2002, Sci, 298, 196
Cox D. P., 1972, ApJ, 178, 143
Cox D. P., Raymond J. C., 1985, ApJ, 298, 651
Croston J. H., Kraft R. P., Hardcastle M. J., 2006, preprint (astro-ph/0610889)
Di Salvo T., Done C., Życki P. T., Burderi L., Robba N. R., 2001, ApJ, 547, 1024
Dopita M., Sutherland R. S., 1995, ApJ, 455, 468
Dopita M., Sutherland R. S., 1996, ApJS, 102, 161
Dopita M. A., Binette L., Dodorico S., Benvenuti P., 1984, ApJ, 276, 653
Drew J. E. et al., 2005, MNRAS, 362, 753
Dunn R. J. H., Fabian A. C., Celotti A., 2006, MNRAS, 372, 1741
Erben T. et al., 2005, Astron. Nachrichten, 326, 432
Fender R. P., 2001, MNRAS, 322, 31
Fender R. P., 2006, in Lewin W. H. G., van der Klis M., eds, Compact Stellar X-ray Sources. Cambridge Univ. Press, Cambridge, p. 381
Fender R. P., Gallo E., Jonker P. G., 2003, MNRAS, 343, L99
Fender R. P., Belloni T. M., Gallo E., 2004, MNRAS, 355, 1105
Fender R. P., Stirling A. M., Spencer R. E., Brown I., Pooley G. G., Muxlow T. W. B., Miller-Jones J. C. A., 2006, MNRAS, 369, 603
Fomalont E. B., Geldzahler B. J., Bradshaw C. F., 2001, ApJ, 558, 283
Forman W. et al., 2005, ApJ, 635, 894
Gallo E., Fender R. P., Pooley G. G., 2003, MNRAS, 344, 60
Gallo E., Fender R. P., Kaiser C., Russell D. M., Morganti R., Oosterloo T., Heinz S., 2005, Nat, 436, 819
Green D. A., 2004, Bull. Astron. Soc. India, 32, 335
Hartigan P., Raymond J., Hartmann L., 1987, ApJ, 316, 323
Hartmann D., Burton W. B., 1997, Atlas of Galactic Neutral Hydrogen. Cambridge Univ. Press, Cambridge
Heinz S., 2002, A&A, 388, L40
Heinz S., 2006, ApJ, 636, 316
Heinz S., Reynolds C. S., Begelman M. C., 1998, ApJ, 501, 126
Homan J., Belloni T., 2005, Ap&SS, 300, 107
Homan J., Buxton M., Markoff S., Bailyn C. D., Nespoli E., Belloni, T., 2005, ApJ, 624, 295
Johnson H. M., 1953, ApJ, 118, 370
Kaiser C. R., Alexander P, 1997, MNRAS, 286, 215
Kaiser C. R., Gunn K. F., Brocksopp C., Sokoloski J. L., 2004, ApJ, 612, 332

King D. L., 1985, ING La Palma Technical Notes, 31
Körding E., Fender R. P., Migliari S., 2006, MNRAS, 369, 1451
Kraft R. P., Vázquez S. E., Forman W. R., Jones C., Murray S. S., Hardcastle M. J., Worrall D. M., Churazov E., 2003, ApJ, 592, 129
Krolik J. H., 1999, Active Galactic Nuclei: From the Central Black Hole to the Galactic Environment. Princeton Univ. Press, Princeton, NJ
Lestrade J.-F., Preston R. A., Jones D. L., Phillips R. B., Rogers A. E. E., Titus M. A., Rioja M. J., Gabuzda D. C., 1999, A&A, 344, 1014
Levenson N. A., Kirshner R. P., Blair W. P., Winkler P. F., 1995, AJ, 110, 739
Martí J., Rodriguez L. F., Mirabel I. F., Paredes J. M., 1996, A&A, 306, 449
Massey P., Johnson K. E., Degioia-Eastwood K., 1995, ApJ, 454, 151
Mavromatakis F., Ventura J., Paleologou E. V., Papamastorakis J., 2001, A&A, 371, 300
McClintock J. E., Remillard R. A., 2006, in Lewin W. H. G., van der Klis M., eds, Compact Stellar X-ray Sources. Cambridge Univ. Press, Cambridge, p. 157
McKee C. F., Hollenbach D. J., 1980, ARA&A, 18, 219
Michael E. et al., 2000, ApJ, 542, L53
Migliari S., Fender R., Méndez M., 2002, Sci, 297, 1673
Mirabel I. F., Rodrigues I., 2003, Sci, 300, 1119
Mirabel I. F., Rodríguez L. F., Cordier B., Paul J., Lebrun F., 1992, Nat, 358, 215
Nowak M. A., Wilms J, Heinz S., Pooley G., Pottschmidt K., Corbel S., 2005, ApJ, 626, 1006
Nulsen P. E. J., McNamara B. R., Wise M. W., David L. P., 2005, ApJ, 628, 629
Ogley R. N., Bell Burnell S. J., Fender R. P., Pooley G. G., Waltman E. B., 2000, MNRAS, 317, 158
Osterbrock D. E., 1989, Astrophysics of Gaseous Nebulae and Active Galactic Nuclei. University Science Books, Sausalito, CA
Perryman M. A. C. et al., 1997, A&A, 323, L49
Predehl P., Schmitt J. H. M. M., 1995, A&A, 293, 889
Pun C. S. J. et al., 2002, ApJ, 572, 906
Raymond J. C., 1979, ApJS, 39, 1
Rodríguez L. F., Mirabel I. F., Martí J., 1992, ApJ, 401, L15
Russell D. M., Fender R. P., Hynes R. I., Brocksopp C., Homan J., Jonker P. G., Buxton M. M., 2006, MNRAS, 371, 1334
Schwartz R. D., 1983, ARA&A, 21, 209
Shull J. M., McKee C. F., 1979, ApJ, 227, 131
Spitzer L., 1978, Physical Processes in the Interstellar Medium. Wiley-Interscience, New York, p. 333
Stirling A. M., Spencer R. E., de la Force C. J., Garrett M. A., Fender R. P., Ogley R. N., 2001, MNRAS, 327, 1273
Tudose V., Fender R. P., Kaiser C. R., Tzioumis A. K., van der Klis M., Spencer R., 2006, MNRAS, 372, 417
Vancura O., Blair W. P., Long K. S., Raymond J. C., 1992, ApJ, 394, 158
Wilson A. S., Smith D. A., Young A. J., 2006, ApJ, 644, L9
Wu C.-C., Holm A. V., Eaton J. A., Milgrom M., Hammerschlag-Hensberge G., 1982, PASP, 94, 149
Xu J-W., Zhang X-Z., Han J-L., 2005a, Chinese J. Astron. Astrophys., 5, 165
Xu J-W., Zhang X-Z., Han J-L., 2005b, Chinese J. Astron. Astrophys., 5, 442

This paper has been typeset from a TEX/LATEX file prepared by the author.